Measurement of the neutron capture cross sections of rhenium up to stellar *s*- and *r*-process temperatures at the China Spallation Neutron Source Back-n facility

Gaole Yang,[1,2] Zhendong An,[1,2,3,4,5,*] Wei Jiang,[6,7] Xiankai Li,[8,2] Weiwei Qiu,[9,3,4] Zhengfa Liao,[9,3,4] Ziyue Zhuang,[9,3,4] Xiaoping Zhang,[3,4,†] Shengli Chen,[9] Chenchen Guo,[9] Erxi Xiao,[9] Xiao Fang,[9] Xinxiang Li,[8,5,10] Hongwei Wang,[5,10,11] Xinrong Hu,[5,10] Bing Jiang,[5,10] Wenqing Shen,[5,11] Jincheng Wang,[12] Jie Ren,[12] Xichao Ruan,[12] Dexin Wang,[13,14] Su-Yalatu Zhang,[13,14] Wen Luo,[8] Zhichao Zhu,[8] Haoyang Lan,[8] Zongwei Cao,[8] Xu Ma,[15,12] Yingdu Liu,[15] Pusen Wang,[15] Yi Yang,[16] Ping Su,[16] Xiangai Deng,[16] Wanbing He,[16] Yugang Ma,[16,5] Chunwang Ma,[17,18] Yuting Wang,[17,18] Zhitao Dai,[19] Ertao Li,[20] Pengqin He,[2] RenGuang Tang,[2] Tao Zhou,[2] Jing Wang,[2] Han Yi,[6,7] Yue Zhang,[6,7] Yonghao Chen,[6,7] Ruirui Fan,[6,7] Keqing Gao,[6,7] Qiang Li,[6,7] Kang Sun,[6,7] Zhixin Tan,[6,7] Minhao Gu,[6,7] Hantao Jing,[6,7] and Jingyu Tang[21,6,7]
(The CSNS Back-n Collaboration)

[1]*Institute of Modern Physics, Chinese Academy of Sciences, Lanzhou 730000, China*
[2]*School of Physics and Astronomy, Sun Yat-sen University, Zhuhai 519082, China*
[3]*State Key Laboratory of Lunar and Planetary Sciences, Macau University of Science and Technology, Macau 999078, China*
[4]*CNSA Macau Center for Space Exploration and Science, Macau 999078, China*
[5]*Shanghai Institute of Applied Physics, Chinese Academy of Sciences, Shanghai 201800, China*
[6]*Institute of High Energy Physics, Chinese Academy of Sciences, Beijing 100049, China*
[7]*Spallation Neutron Source Science Center, Dongguan 523803, China*
[8]*School of Nuclear Science and Technology, University of South China, Hengyang 421001, China*
[9]*Sino-French Institute of Nuclear Engineering and Technology, Sun Yat-sen University, Zhuhai 519082, China*
[10]*University of Chinese Academy of Sciences, Beijing 100049, China*
[11]*Shanghai Advanced Research Institute, Chinese Academy of Sciences, Shanghai 201210, China*
[12]*Key Laboratory of Nuclear Data, China Institute of Atomic Energy, Beijing 102413, China*
[13]*College of Mathematics and Physics, Inner Mongolia Minzu University, Tongliao 028000,China*
[14]*Institute of Nuclear Physics, Inner Mongolia Minzu University, Tongliao 028000, China*
[15]*Shool of Materials Science and Engineering, Xiangtan University, Xiangtan 411100, China*
[16]*Key Laboratory of Nuclear Physics and Ion-beam Application (MOE), Institute of Modern Physics, Department of Nuclear Science and Technology, Fudan University, Shanghai 200433, China*
[17]*Institute of Particle and Nuclear Physics, Henan Normal University, Xinxiang 453007, China*
[18]*School of Physics, Henan Normal University, Xinxiang 453007, China*
[19]*Shenzhen Center, Cancer hospital, Chinese Academy of Medical Sciences, Shenzhen 518100, China*
[20]*Institute for Advanced Study in Nuclear Energy and Safety, College of Physics and Optoelectronic Engineering, Shenzhen University, Shenzhen 518060, China*
[21]*School of Nuclear Science and Technology, University of Science and Technology of China, Hefei 230027, China*

(Received 14 June 2023; accepted 9 October 2023; published 1 March 2024)

The neutron capture measurement of natural rhenium was performed with the time-of-flight technique at the Back-n facility of the China Spallation Neutron Source in the energy range from 1 to 500 eV of the resolved resonance region (RRR) and from 5 to 400 keV in the unresolved resonance region (URR). Prompt γ-rays originating from neutron-induced capture events were detected by four C_6D_6 detectors. The pulse height weighting technique and the double-bunch unfolding method based on the Bayesian theory were used in the data analysis. To obtain reliable measurement results, background subtraction, normalization, and corrections were carefully considered. The multilevel R-matrix Bayesian code SAMMY was used to extract the resonance parameters in the RRR. An absence of resonance near 392 eV is observed in our measurement, which has been observed in previous works. The average cross sections in the URR of natural rhenium relative to ^{197}Au were obtained in logarithmical equidistant energy bins with 20 bins per energy decade. The TALYS code was used to describe the average cross sections in the URR; the Maxwellian-averaged cross sections (MACSs) of ^{185}Re and ^{187}Re are given from $kT = 5$ to 100 keV. At a thermal energy of $kT = 30$ keV, the MACS value for ^{185}Re (1469 ± 127 mb) is in good agreement with the Karlsruhe Astrophysical Database of Nucleosynthesis in Stars

*anzhendong@sinap.ac.cn;
†xpzhang@must.edu.mo;

(KADoNIS) recommended value (1535 ± 62 mb) within the error bars. By contrast, the value of 1361 ± 118 mb for ^{187}Re shows a discrepancy with the KADoNiS recommended value (1160 ± 57 mb).

DOI: 10.1103/PhysRevResearch.6.013225

I. INTRODUCTION

Rhenium is almost the rarest element in the earth's crust. Rhenium has the highest boiling point (5590 °C) among all elements and a high melting point (3185 °C [1]). Being a refractory metal, rhenium has a good resistance to heat and wear as well as an excellent ductility at lower temperatures. Tungsten or molybdenum alloys containing rhenium have the desirable alloying characteristics for use in high-temperature power reactors, including space fission reactors and fusion reactors [2–5]. In these applications, more accurate and reliable experimental data on the neutron-induced reaction are required for its design and optimization.

Natural rhenium contains two isotopes, the stable isotope ^{185}Re (37.4%) and the long-lived isotope ^{187}Re (62.6%), which has a half-life of $4.12(\pm 0.13) \times 10^{10}$ years [6]. Long-lived radioactive nuclei are promising for use as nucleochronometers in the investigation of the nucleosynthesis process in studies on the universe's history. The ^{187}Re–^{187}Os pair is one of the rarest cosmological nucleocosmochronometers with half-lives in the range of the cosmic age, 1–100 Gyr [7]. Numerous studies on the nucleosynthesis process of the region around tungsten, rhenium, and osmium have been conducted in recent years [8–10]. In Fig. 1, we illustrate the nucleosynthesis processes in this region [9,10]. The stable and long-lived nuclei are indicated by the black boxes, whereas the unstable nuclei are marked by the green boxes. The black and blue solid lines represent the main *s* and *r* processes, respectively, and the black dashed lines denote the weaker secondary processes, and the red dashed line represents the β-decay of long-lived ^{187}Re. The ^{187}Re nucleus is located outside the main *s*-process chain; thus, the nucleosynthesis of ^{187}Re is predominantly attributed to the *r* process. Due to the shielding of the stable and long-lived isobars ^{186}W and ^{187}Re, ^{186}Os, and ^{187}Os are eliminated from the β-decay chains of the *r* process; thus, they can be regarded as *s*-only isotopes, as indicated by the *s* label in Fig. 1. The nucleosynthesis phenomena occurring in this region can be used as a cosmological clock to record the time at which an *r*-process nucleosynthesis event occurs. On the timescale of the universe, the *s*-only nucleus ^{187}Os is also produced in large quantities by the radiogenic decay of ^{187}Re. Thus, abundance of ^{187}Os includes the *s*-process component and the radiogenic component; the latter is essential for evaluating the epoch of an *r*-process nucleosynthesis event and can be calculated by subtracting the *s*-process component from the total abundance. The *s*-process component can be calculated through the nucleosynthesis model and normalized by the abundance of the *s*-only isotope ^{186}Os. For a detailed analysis of the nucleosynthesis reaction flow in this region, larger data sets and more accurate measurement data on the neutron-induced reaction, especially the Maxwellian-averaged cross sections (MACSs) for neutron capture in the keV region, are required.

Previous neutron capture cross-section ($\sigma_{n\gamma}$) measurements of natural rhenium are shown in Fig. 2(b); most of these involve the energy range from 1 keV to 1 MeV. In 1961, Block [11] measured the neutron capture cross section of natural rhenium ($\sigma_{n\gamma}$) from 210 to 9450 eV using the time-of-flight (TOF) method. In 1963 [12] and 1987 [5], Macklin and coworkers performed the neutron capture cross section measurements at the Oak Ridge National Laboratory in the unresolved resonance region (URR). In 1971, Bergman *et al.* [13] measured the capture cross section in both the resolved resonance region (RRR) and the URR using the slowing-down-time-in-lead method. More recently, Epping *et al.* [4] measured the neutron transmission yield and capture yield of natural rhenium from 1 to 600 eV in the RPI LINAC facility. In Fig. 2(a), we illustrate the most recently evaluated capture cross sections ($\sigma_{n\gamma}$) of natural rhenium [14–17]. They are obtained from the isotopic cross section ($\sigma_{n\gamma}$) of ^{185}Re, ^{187}Re, and their abundances. These values are in good agreement with each other in the RRR. By contrast, they have clear discrepancies in the URR.

Our work was performed at the back-streaming white neutron beam line (Back-n) of the China Spallation Neutron Source (CSNS) [24,25]. The deexcited γ rays were detected by four hydrogen-free deuterated benzene (C_6D_6) liquid scintillator detectors [26] and the pulse height weighting technique (PHWT) was used to correct the efficiencies of the γ-ray detection. A ^{6}LiF–Si detector array [27] was used as a neutron flux monitor to provide in-line neutron monitoring and the neutron flux profile. The data analysis was divided into the RRR from 1 to 500 eV and the continuum part from 5 to 300 keV. The *R*-matrix code SAMMY (version M6) [28,29]

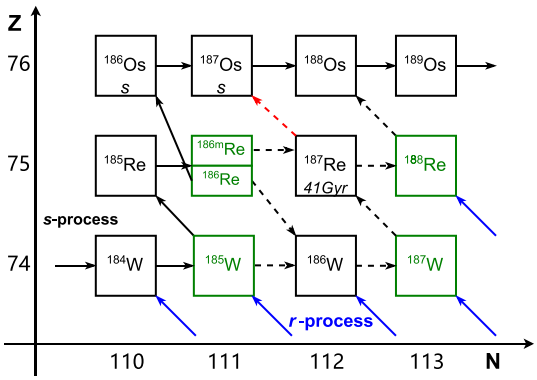

FIG. 1. Nucleosynthesis processes occurring in the region among tungsten, rhenium, and osmium. The *s* and *r* processes are indicated by black and blue arrows, respectively. The stable (unstable) and long-lived nuclei are marked by black (green) boxes, with the dashed lines indicating weaker secondary processes. The decay of ^{187}Re shown by the dashed red arrow represents a cosmochronometer.

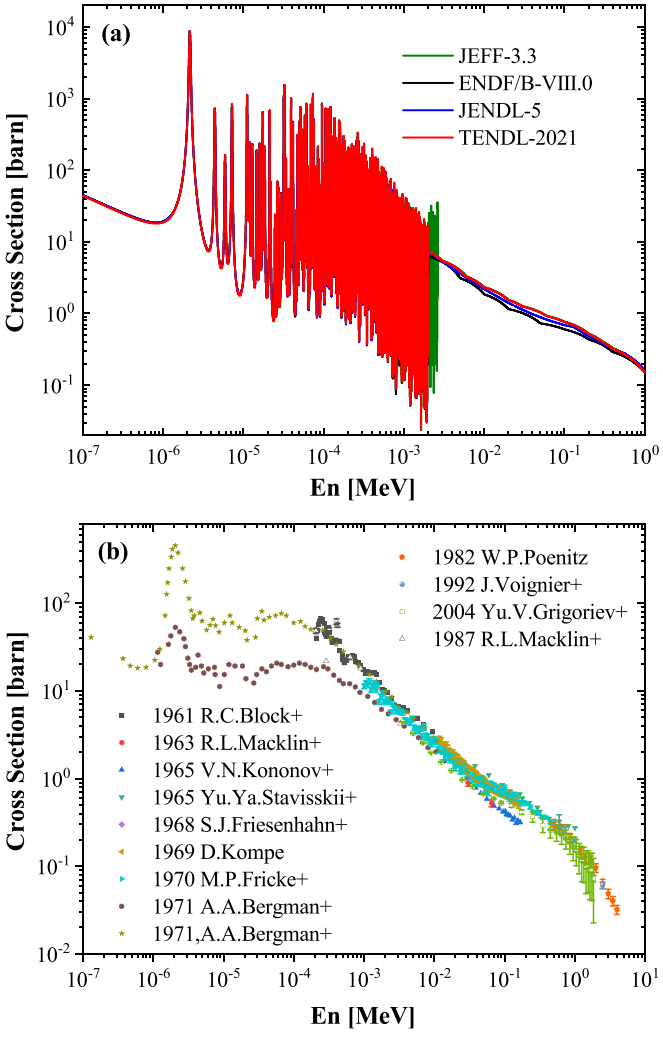

FIG. 2. (a) Evaluated cross sections of ^{nat}Re (n, γ), including ENDF/B-VIII.0 [14], TENDL-2021 [16], JENDL-5 [15], and JEFF-3.3 [17]. (b) Previous experimentally measured cross sections of ^{nat}Re (n, γ) compiled in the EXFOR database [5,11–13,18–23].

was used to normalize the experimental yields with the 4.9 eV resonance of ^{197}Au sample. SAMMY was still used to extract the resonance parameters in the RRR, while the data in the URR were analyzed using the TALYS (version 1.96) [30,31] code.

The experimental conditions of the Back-n facility used in this paper and the corresponding experimental setup are presented in Sec. II. The data analysis is stated in Sec. III, including the PHWT, double-bunch unfolding method, background subtraction, normalization, and corrections. The theoretical description of our experimental results, which was performed using the SAMMY and TALYS codes for the RRR and the URR, respectively, is discussed in Sec. IV. Finally, the conclusions are drawn in Sec. V.

II. MEASUREMENTS

A. The Back-n facility at CSNS

CSNS was the first spallation neutron source facility in China [24]. A white neutron beamline (Back-n) was

FIG. 3. Photograph of the C_6D_6 detector system in the Back-n facility of CSNS; a gold sample is placed in the aluminum sample holder.

constructed in the direction of 180° related to the proton beam of the CSNS [25]. The main objectives of the experimental activity of the Back-n facility are nuclear data measurements, basic nuclear physics, particle physics, neutron radiation measurements, and neutron photography. Regarding the nuclear data measurements, the Back-n facility focuses on the accurate measurement of the neutron cross sections ($\sigma_{n\gamma}$) related to nuclear astrophysics and the collection of nuclear data related to emerging nuclear technologies for energy production, such as thorium-based molten salt reactors, research and development of accelerator-driven systems (ADSs), and nuclear-waste transmutation [25,32]. During phase I of the CSNS [25], a 1.6 GeV/c proton beam with a power up to 100 kW bombards a tantalum-cladded and water-cooled sliced tungsten target (W–Ta target) at a repetition rate of 25 Hz; the primary neutrons generated during this spallation process are slowed by three neutron moderators, providing a pulsed neutron beam with an energy ranging from the thermal energy to 200 MeV [24]. There are two experimental stations (ESs) in the Back-n beamline, namely, ES No. 1 and ES No. 2. ES No. 2 is located at approximately 76 m from the spallation target, in which the neutron flux can reach 10^7 n/cm^2/s. ES No. 2 is mainly used for measuring the cross sections of the (n, γ) [33–35], (n, tot), and (n, f) reactions and our experiments were carried out here. A detailed description of the facility and its characteristics can be found in Refs. [25,32].

In the Back-n beamline, the neutron beam is shaped by a neutron shutter located 20 m from the spallation target and two collimators located at the front end of ES No. 1 and ES No. 2 [25]. The detector system for the $\sigma_{n\gamma}$ measurement consists of four C_6D_6 detectors, the aluminum detector brackets, and an aluminum sample holder [26], as shown in Fig. 3. The C_6D_6 detectors are placed upstream of the sample and the detector axis is at an angle of 110° relative to the neutron beam. The distance between the front center of the C_6D_6 detectors and the sample target center is 150 mm, while it is 80 mm between the front center of the C_6D_6 detectors and the neutron beam axis. A neutron conversion layer consisting of a

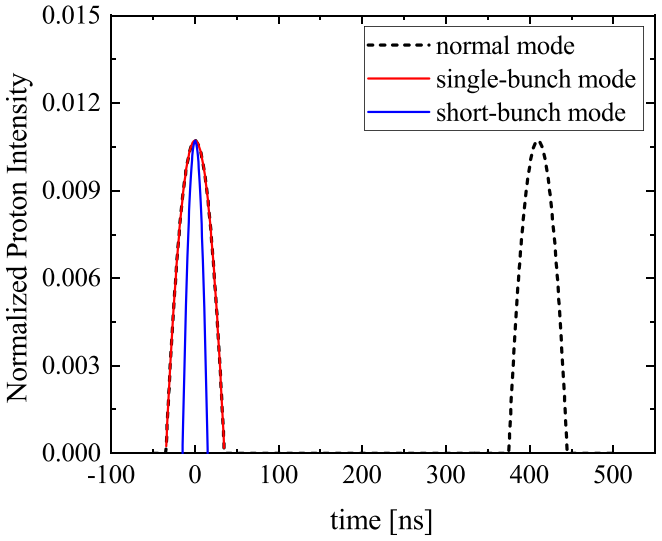

FIG. 4. Proton flux intensity distributions of the normal mode, single-bunch mode, and short-bunch mode in CSNS [25].

360 μg/cm^2 ^{6}LiF film deposited on a 10-μm-thick aluminum foil is placed in the neutron beam line at the front end of ES No. 1 and is part of a ^{6}LiF–Si detector array with eight separated Si detectors [27]. Signals from these detectors are processed by a generalized full waveform digital data acquisition system [25]. A generalized readout electronics with 64 channels was constructed based on the PXIe frame for data acquisition in the Back-n beamline, in which the flash analog-to-digital converters are based on the folding-ADC and FPGA techniques. Each channel has a digital resolution of 12 bits and a sampling rate of 1 GSPS, corresponding to a time step of 1 ns/sample. The digital waveform data of the detectors are filtered by a full-digital trigger system and then transferred to the CSNS computation center for long-term storage.

B. Experimental setup

Our work was carried out at ES No. 2. A thin foil of a cadmium absorber was placed at the front of the neutron shutter to absorb neutrons with an energy lower than 0.5 eV for avoiding the overlapping between consecutive neutron pulses. In addition, a Ta–Ag–Co filter with a total thickness of 1.0+0.4+1.4 mm was used to determine the in-beam γ-ray background by employing the black resonance method. For our measurements, the shutter and collimators had an inner diameter of $\phi 50 + \phi 15 + \phi 40$ mm, resulting in a circular Gaussian-shaped beam profile with a diameter of around 40 mm at the sample position. CSNS provides three types of proton beam operation modes [25], namely, the normal operation mode (i.e., the double-bunch operation mode), single-bunch operation mode, and short-bunch operation mode, as shown in Fig. 4. Our experiments were performed under the normal operation mode [36,37], in which the accelerator delivers a proton beam with two bunches separated by 410 ns in a pulse to produce a higher neutron flux and reduce the required experimental time. Additional problems are posed by this mode for the TOF measurements and data analysis; thus, a so-called unfolding method was developed to deconvolute the two bunches in one pulse [38]. The details of this method will be discussed in Sec. III.

A total of four samples were used in the measurements: (i) a natural rhenium sample under study, (ii) a ^{197}Au sample for experimental setup verification and flux normalization, (iii) a natural carbon sample, and (iv) a lead sample used to determine the backgrounds due to scattered neutrons and the in-beam γ rays. In the experiments, the samples were fixed on the aluminum sample holder of the C_6D_6 detector system. The characteristics of the samples and the experimental duration are summarized in Table I.

III. DATA ANALYSIS

The data analysis was divided into the RRR and the continuum URR. The parameters in the RRR were obtained up to neutron energies of 500 eV, while those in the URR were obtained from 5 to 300 keV.

The PHWT and the double-bunch unfolding method based on the Bayesian theory were used to preprocess the experimental data. The capture data were obtained from the preprocessed data after background subtraction and flux normalization. In the URR, to obtain more reliable results, the data were corrected to take into account multiple scattering events and self-shielding using the GEANT4 TOOLKIT [39] (version 10.4.p01) and FTFP_BERT_HP physics list. Finally, the average capture cross sections are given relative to ^{197}Au.

A. PHWT

The efficiency of the C_6D_6 detectors depends on the energy of the incident γ rays. Thus, the C_6D_6 detector's record counts of cascading emitted γ rays from the neutron capture events depend on the deexcitation paths of the compound nucleus, which are too complex to calculate the actual number of capture events [26]. To obtain the actual experimental capture yields, an *a posteriori* manipulation on the detector's raw counts is proposed [26] which will ensure that the γ-ray

TABLE I. Characteristics of the samples and experimental duration of our experiments.

					Experimental duration (h)	
Target	Mass (g)	Diameter (mm)	Thickness (mm)	Purity (%)	Without filter	With filter
Gold	4.83 ± 0.01	40.0 ± 0.02	0.20 ± 0.02	⩾99.9	13.0	4.0
Rhenium	13.76 ± 0.01	40.0 ± 0.02	0.50 ± 0.02	⩾99.9	11.5	3.5
Lead	13.93 ± 0.01	40.0 ± 0.02	0.98 ± 0.02	⩾99.9	8.0	
Carbon	2.86 ± 0.01	40.0 ± 0.02	1.02 ± 0.02	⩾99.9	8.7	
Empty					8.0	6.0

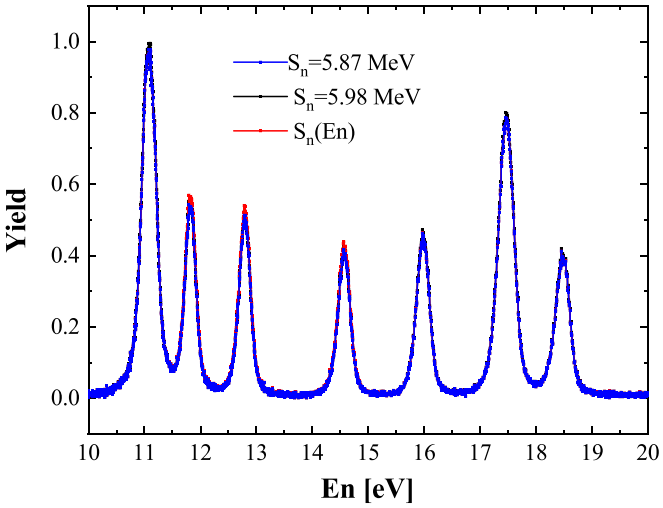

FIG. 5. Results of experimental yields obtained with three types of S_n value. For comparison, error bars are not shown in this figure.

efficiency ϵ_γ increases linearly with the energy of the incident γ rays, E_γ, that is,

$$\epsilon_\gamma = c \cdot E_\gamma, \tag{1}$$

where c is a proportionality coefficient. The capture efficiency ϵ_c, which represents the probability to detect at least one cascading emitted γ ray from a single neutron capture event, can be expressed as

$$\epsilon_c = 1 - \prod_{i=1}^{N}(1 - \epsilon_{\gamma i}),$$

where the subscript γi represents each cascading emitted γ ray of the capture event. According to Eq. (1), when ϵ_γ is sufficiently low ($\epsilon_\gamma \ll 1$), this equation can be rewritten as

$$\epsilon_c \simeq \sum_{i=1}^{N} \epsilon_{\gamma i} = c \sum_{i=1}^{N} E_{\gamma i} = c \cdot (S_n + E_n), \tag{2}$$

where $E_{\gamma i}$ is the ith cascading γ ray's energy, S_n is the neutron binding energy of the compound nuclei, and E_n is the kinetic energy of an incident neutron in the center of the mass system. This equation indicates that the capture efficiency ϵ_c is independent of the actual deexcitation path. In this paper, $S_n = 6.18$ MeV and 5.87 MeV for ^{185}Re and ^{187}Re, respectively. However, only a single S_n can be used in Eq. (2). We compared three different ways of choosing the S_n value: (i) method from Ref. [40]—choose the S_n value of the isotope with the highest abundance in the target (^{187}Re in this case with $S_n = 5.87$ MeV); (ii) method from Ref. [41]—weighted average S_n value according to their isotopic abundances in target ($S_n = 5.98$ MeV); and (iii) average S_n value weighted by their theoretical capture yields (calculated with ENDF/B-VIII.0 database), which is a function of neutron energy (E_n) rather than a constant. Yields from these different ways are shown in Fig. 5—the systematic uncertainty caused by the choosing of S_n is less than 3%. Finally, the method in Ref. [40] is applied in this paper, and the abundance of the ^{185}Re isotope in the target is scaled according to its S_n value in subsequent SAMMY resonance shape analysis.

The PHWT was found to achieve this manipulation, in which the detector count of each depositional energy is multiplied by a weighting function (WF) to correct for the original γ-ray efficiency of the detectors, so the relationship expressed in Eq. (1) is achieved. In this paper, a realistic Monte Carlo simulation of the experimental conditions and the target setup was performed using the GEANT4 toolkit and was used to calculate the WFs. The WFs are parametrized as fourth stairs polynomial functions of the γ-ray energy, that is,

$$\mathrm{WF}(E_d) = \sum_{k=0}^{4} a_k E_d^k, \tag{3}$$

where E_d is the energy deposited in the C_6D_6 detectors. A least-squares method is used to determine the WFs according to

$$\chi^2 = \sum_i \left(cE_{\gamma i} - \int_{E_L}^{\infty} R(E_d, E_{\gamma i}) WF(E_d) \mathrm{d}E_d \right)^2, \tag{4}$$

where E_L is the low deposited energy threshold of the C_6D_6 detector, and $R(E_d, E_{\gamma i})$ is the detector response function for monoenergetic γ rays generated from the target surface and is obtained via GEANT4 Monte Carlo simulations. The WFs of the natural rhenium and gold samples were determined independently using this method. Twenty groups of simulated monoenergetic γ rays with energies ranging from 0.15 to 9 MeV were produced from the volume (surface) of the natural rhenium and gold samples; furthermore, part of the gamma ray energy was deposited on the C_6D_6 detectors as shown in Fig. 6. A detailed study of the possible sources of systematic uncertainties revealed that the PHWT has an accuracy of 3% [42,43].

B. Double-bunch unfolding method

At present, the accelerator complex of CSNS operates in the normal mode; each pulse contains two proton bunches and the interval between the two bunches is 410 ns [25]. The neutrons generated by the two proton bunches overlap with each other. Thus, the neutron energy resolution of the TOF measurement is reduced, especially in the higher-neutron-energy region (above hundreds of eV). An unfolding method based on Bayes' theorem was developed by Yi *et al.* [44] to obtain better time and energy resolution.

As shown in Fig. 4, in the normal mode of CSNS, the two bunches in each single beam pulse are basically identical, and the temporal structure is extremely reproducible from pulse to pulse; the details can be found in Refs. [25,44]. For the statistical time count spectrum measured in the normal mode, the counts of each time bin E_i measured in such a mode should depend on the counts C_i measured in the single-bunch mode. Theoretically, the single-bunch spectrum can also be unfolded from the double-bunch spectrum, where the unfolding problem can be treated as an inverse matrix problem [44]. Based on Bayes' theorem, the inverse matrix problem can be solved in an iterative process [44,45],

$$\bar{C}_i^{k+1} = E_i \frac{C_i^{(k)}}{C_{i-\Delta}^{(k)} + C_i^{(k)}} + E_{i+\Delta} \frac{C_i^{(k)}}{C_i^{(k)} + C_{i+\Delta}^{(k)}}, \tag{5}$$

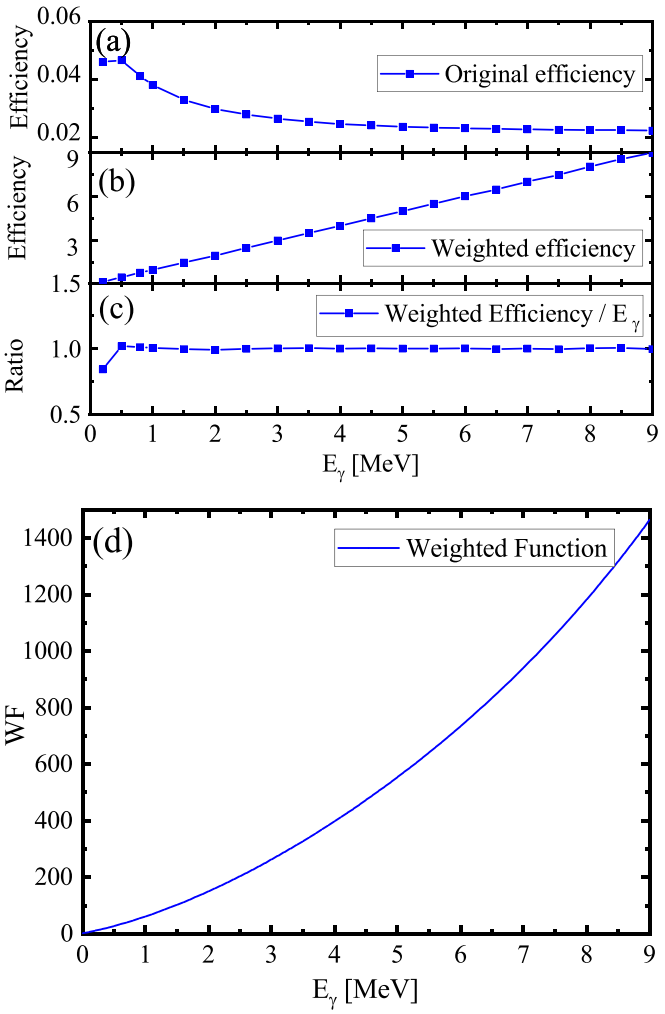

FIG. 6. (a) Original efficiency of the C_6D_6 detector; (b) Efficiency of the detector weighted by the WF; (c) coefficient of the weighted efficiency vs incident γ ray's energy; (d) WF of the C_6D_6 detector.

where $C_i^{(k)}$ indicates the single-bunch distribution obtained in the kth iteration and Δ is the number of bins corresponding to the offset of the double-bunch interval (410 ns). According to the convergence theory of an iterative algorithm, the final distribution is independent of the initial distribution; thus, the initial $C_i^{(0)}$ is always set as the E_i measured in the double-bunch distribution. In iterative Eq. (5), error propagation of statistical uncertainties from the double-bunch spectrum also be considered, as detailed in Ref. [44]. This method was verified with the gold sample, as illustrated in Fig. 7.

C. Background

The original spectra preprocessed using the PHWT and the double-bunch unfolding method were normalized by the proton beam number and are shown in Fig. 8.

To obtain the actual counts of the rhenium radiation capture reaction, it is necessary to subtract various backgrounds, including the neutron-induced background and in-beam γ-ray background, etc. According to sample correlation, the background in our measurements can be

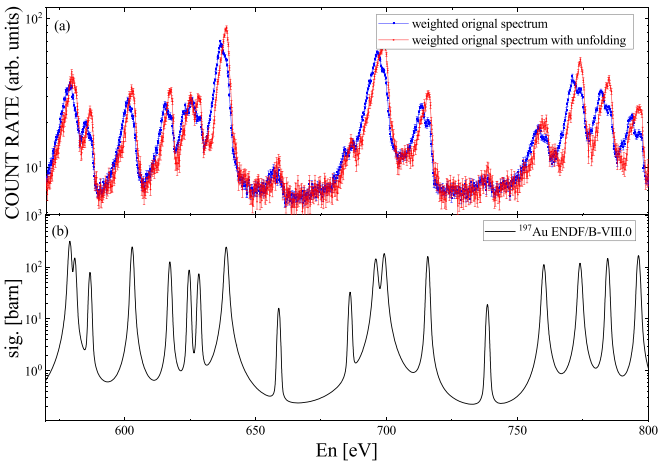

FIG. 7. (a) Comparison between the weighted original spectrum of the gold sample (blue curve) and the weighted original spectrum obtained from the unfolding process (red curve); (b) ENDF/B-VIII.0 database [14] of gold. In panel (a), the blue curve shows the presence of clear double peaks caused by the double-bunch mode, while the resonance structures are restored when using the unfolding procedure, as indicated by the red curve.

divided into a sample-dependent background $B_{\text{sample}}(t_n)$ and sample-independent background $B_{\text{empty}}(t_n)$ [36,37,46], that is,

$$B(t_n) = B_{\text{empty}}(t_n) + B_{\text{sample}}(t_n). \tag{6}$$

The contribution of $B_{\text{empty}}(t_n)$ can be directly measured in the same experimental setup by keeping the sample away from the neutron beam. On the other hand, the sample-dependent background $B_{\text{sample}}(t_n)$ is caused by interactions between the sample and all types of in-beam particles, including the scattered-neutron-induced background $B_{sn}(tn)$, scattered in-beam γ-ray background $B_{s\gamma}(t_n)$, and sample activation background $B_{ac.}$. Thus, the sample-dependent background can

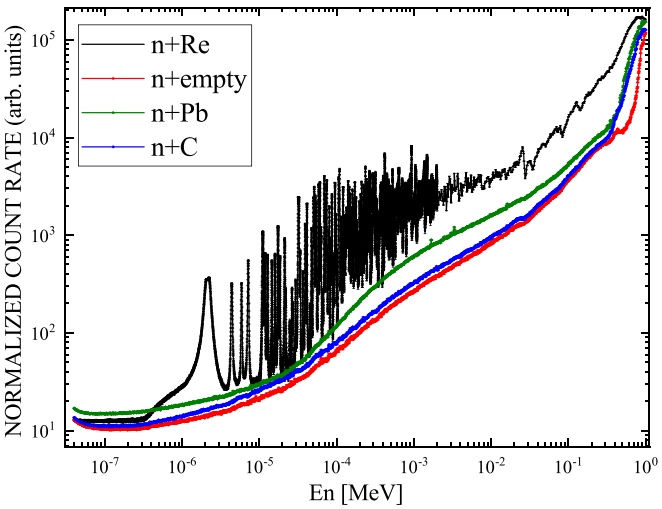

FIG. 8. Preprocessed and normalized (according to the proton beam number) original spectra of ^{nat}Re, ^{nat}C, ^{nat}Pb, and the empty target.

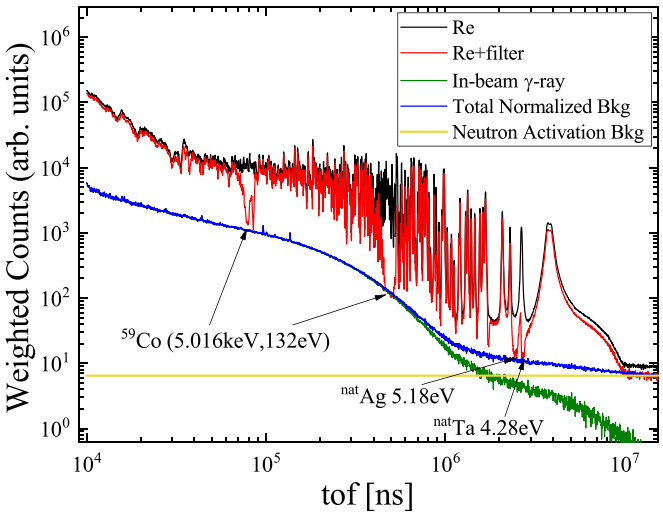

FIG. 9. The measured in-beam γ-ray backgrounds were normalized to match the valleys caused by the black resonances, namely, with energy 4.28 eV (Ta filter), 5.18 eV (Ag filter), and 132 eV and 5.016 keV (Co filter).

be expressed as [46]

$$B_{\text{sample}}(t_n) = B_{sn}(t_n) + B_{s\gamma}(t_n) + B_{ac}. \tag{7}$$

As the cross sections of the neutron-scattering-induced and γ-ray-induced interactions vary considerably depending on the nucleus, the sample-dependent background $B_{\text{sample}}(t_n)$ can hardly be determined through direct measurements. Thus, measurements of carbon and lead samples as well as the black resonance method were introduced to determine these backgrounds; the validity of these methods was verified through GEANT4 simulations in Ref. [47].

The neutron capture cross section of carbon is considerably smaller than the scattering cross section, and the carbon scattering of γ rays is very weak. These characteristics indicate that the carbon sample can be used to determine the scattered-neutron-induced background $B_{sn}(t_n)$ as

$$B_{sn}(t_n) = \frac{Y_{\text{Re,el}}}{Y_{\text{C,el}}}(W.C_C(t_n) - W.C_{\text{empty}}(t_n)), \tag{8}$$

where $Y_{\text{C,el}}$ and $Y_{\text{Re,el}}$ are the neutron scattering yields of the carbon and rhenium targets obtained from the database. The in-beam γ rays originated from neutron captures in the water moderators of the spallation source. Indeed, these γ rays can be scattered by the sample. The target and energy dependence of in-beam γ-ray background components were determined from a dedicated measurement of a lead sample and the absorption valleys of 4.28 eV, 5.18 eV, 132 eV, and 5.02 keV of the Ta–Ag–Co filter, as shown in Fig. 9.

In this figure, the empty background $B_{\text{empty}}(t_n)$ is subtracted from all spectra, and the background due to the scattered neutrons from lead sample is subtracted using Eq. (8). The figure also shows the activation background, which is determined by fitting the spectra's platform above 11 ms ($E_n \approx 0.2$ eV). In this region, neutrons are absorbed by the cadmium absorber, and the in-beam γ-rays can be ignored; the counts in the residual TOF spectrum are attributed to the activation of the sample and the surrounding materials.

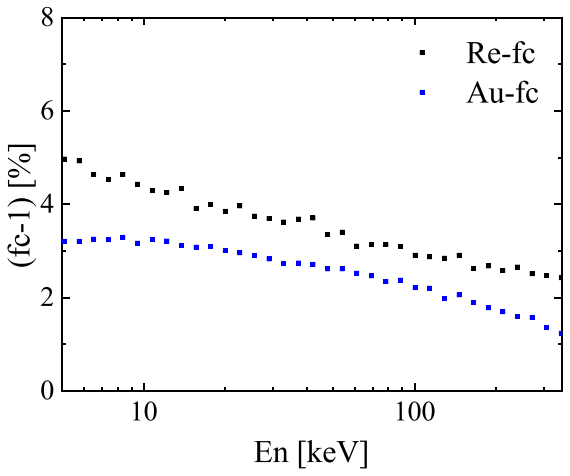

FIG. 10. Correction factor for the multiple scattering events and the self-shielding effect calculated using the GEANT4 toolkit: The black solid dots represent natural rhenium, while the red solid dots represent the gold sample.

D. Experimental corrections

In the RRR, sample-related corrections were included in the SAMMY analysis. In the URR, neutron multiple scattering events and self-shielding corrections in the sample were determined through GEANT4 simulations, that is,

$$\sigma_\gamma = \frac{N_w}{IS_n} \times \frac{\sigma_t}{1 - \exp N f_c t \sigma_t}, \tag{9}$$

where f_c is the correction factor for the multiple scattering events and the self-shielding [33], and ρ is the area density in atom/barn of the sample, which is 0.00339 atom/barn for the rhenium sample and 0.00117 atom/barn for the gold sample as shown in Fig. 10.

E. Absolute neutron flux

A relative normalization of the well-defined energy dependence of the neutron flux could be obtained for the various runs via the Li–Si neutron detectors [27] in ES No. 1. The absolute flux was determined by means of the gold reference sample using the (n, γ) cross section of ^{197}Au as a standard [22,29,48].

The first gold resonance at 4.9 eV was used to define the flux in the RRR using the saturated resonance method, as shown in Fig. 11. The absolute yield normalization was determined through a fit of the gold target's data using the R-matrix code SAMMY and by adopting the resonance parameters of Ref. [48]. In the keV region, the average (n, γ) cross sections were obtained relative to gold. The background of the Au spectrum was determined using the same method adopted for the rhenium spectra.

F. Discussion of the uncertainties

The total uncertainties, including statistical and systematic, will be discussed. The statistical uncertainty comes from raw counts in a energy bin of four samples and was estimated to be <2.0%. In fact, the raw counts will change depending on the width of energy bins and value of (n, γ) cross sections.

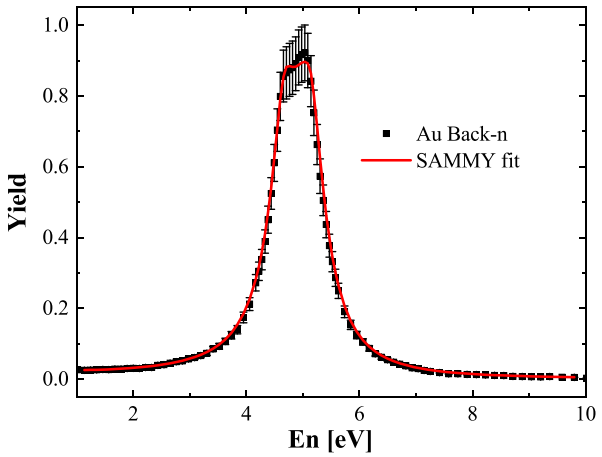

FIG. 11. Capture yield of the first resonance (4.9 eV) of ^{197}Au measured at the Back-n facility and normalized by the SAMMY fit.

Wider energy bins will help to increase the counts and reduce the statistical error, for energy >2.0 keV, but at the same time, energy bins that are two wide cannot exhibit the fine resonance structure.

The systematic uncertainties are mainly contributed by the uncertainty of experimental conditions and data analysis method. Uncertainty of experimental conditions contains several types, including uncertainty of sample parameter, neutron energy spectrum, and proton beam power. Uncertainty of the data analysis method is mainly caused by the PHWT method, double-bunch unfolding process, normalization, background subtraction, and correction in the URR. Finally, according to the error propagation, the overall experimental uncertainty is less than 10.0% in Table II. Such a high error mainly comes from the uncertainty of the neutron spectrum (<8%). Therefore, a good neutron energy spectrum with lower uncertainty will greatly improve the accuracy of this experiment.

IV. RESULTS AND DISCUSSION

A. R-matrix fits

In the RRR from 1 to 500 eV, the natural rhenium capture yields were analyzed using the R-matrix code SAMMY. The yield was parametrized via the multilevel *R*-matrix theory with the Reich-Moore approximation using a channel radius of 8.70 fm [49] and a temperature of 293 K for the correction of the Doppler effect. The multiple neutron scattering events in the sample and the neutron self-shielding were properly taken into account within the SAMMY code. The resonance broadening due to the neutron energy resolution function was also considered in the SAMMY fits through the implemented RPI parametrization [50].

TABLE II. Statistical and systematic errors for rhenium measurement.

Component	Uncertainty (%)
PHWT	3.0
Unfolding method	2.0
Normalization	1.5
Background subtraction	2.0
Experimental corrections	1.0
Proton beam power	1.5
Sample parameters	0.1
Neutron spectrum ($\geqslant$0.15 MeV)	4.5
Neutron spectrum ($\leqslant$0.15 MeV)	8.0
Statistical	2.0

The fitting procedure allowed us to extract the resonance parameters (radiation width Γ_γ, neutron width Γ_n, orbital angular momentum L, etc.) from the measured capture yields. However, in many cases, only the resonance energy E_R and the total capture kernel k should be considered as the real measurable quantities. The capture kernel k is proportional to the area under an isolated resonance and is given by

$$k = g\Gamma_n\Gamma_\gamma/\Gamma, \tag{10}$$

where g is a statistical factor defined as

$$g = \frac{2\boldsymbol{J}+1}{(2\boldsymbol{s}+1)(2\boldsymbol{I}+1)}, \tag{11}$$

where $\boldsymbol{J}$ is the total angular momentum, $\boldsymbol{s}$ is the spin of the incident particles (1/2 for neutrons), and $\boldsymbol{I}$ is the spin of the target particles (5/2 for both ^{185}Re and ^{187}Re).

Resonance parameters compiled in ENDF/B-VIII.0 library for both ^{185}Re and ^{187}Re were used as initial values in SAMMY fits. The final SAMMY fitted results of the natural rhenium capture yield are shown in Fig. 12: the black data represent the rhenium capture yield measured in this paper, and the red solid curve is the SAMMY fitted values to the present data. For comparison, the logarithmic ratios of the kernels obtained from this work and from ENDF/B-VIII.0 is illustrated in Fig. 13.

In region near 390 eV, as shown in Fig. 14, we observed an absence of 391.9 eV resonance compared with previous data [4,51], which is also reported in ENDF/B-VIII.0 and Mughabghab (2006) [49]. Based on the resolution of our experimental facility, such resonance with large neutron width as previously reported [49] should be clearly distinguished from nearby resonances. Hence, we consider its presence unlikely according to experimental data of this work. For comparison with evaluated databases, we calculated neutron capture cross section $\sigma_{\text{exp.}}(\text{n},\gamma)$ of Re with our experimental yield $Y_{\text{exp.}}(\text{n},\gamma)$ [52],

$$\sigma_{\text{exp.}}(n,\gamma) = \frac{Y_{\text{exp.}}(\text{n},\gamma)\sigma_{\text{tot}}}{(1-e^{-N\sigma_{\text{tot}}})}, \tag{12}$$

in which σ_{tot} is the total cross section calculated from the Evaluated Nuclear Data Files (ENDF/B-VIII.0) and N is atomic number density of Re target. Calculated $\sigma_{\text{exp.}}(\text{n},\gamma)$ is plotted with blue dots in Fig. 15.

B. Statistical analysis

The present resonance parameters extracted by SAMMY fit was used for a statistical analysis. A staircase plot of cumulative number of resonances as a function of neutron energy is shown in Figs. 16(a) and 16(b) for ^{185}Re and ^{187}Re, respectively, which provide an efficient way to investigate

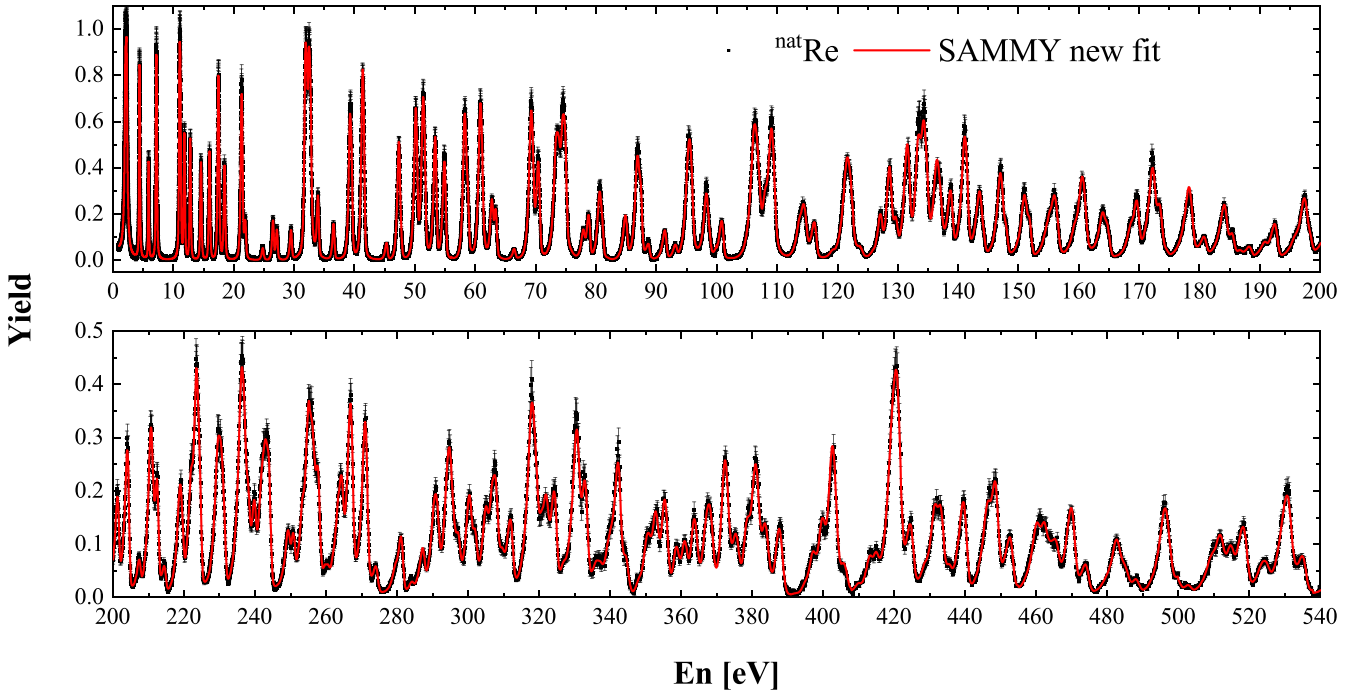

FIG. 12. Analysis of the resonance parameters of the experimental data fitted by the R-matrix code SAMMY.

average level spacing D_0 and missing levels. Average level spacing D_0 is the inverse of the slope of straight line obtained by linear least-squares fits to each staircase line, which is 3.144 eV and 3.903 eV for ^{185}Re and ^{187}Re, respectively. Based on Dyson-Mehta statistical theory of neutron capture levels [53], points fall below the fitted straight line, indicating that levels are being missed in the resonance analysis. In this case, staircase lines near 500 eV for both ^{185}Re and ^{187}Re are below fitted straight line, which means some very weak resonances and unresolved doublets may exist in this energy region. In addition, the average radiative widths $\langle\Gamma_\gamma\rangle$ are calculated with SAMMY fitted resonance parameters, which is 58.9 ± 2.3 meV and 62.6 ± 2.5 meV for ^{185}Re and ^{187}Re, respectively.

C. MACSs

In the URR, the averaged cross section $\sigma_{\mathrm{Re}}(E_{\mathrm{n}})$ is given in relation to the gold sample, according to

$$\sigma_{\mathrm{Re}}(E_{\mathrm{n}}) = \frac{\sigma_{\mathrm{Au}}(E_{\mathrm{n}})}{\langle\sigma_{\mathrm{Au}}(E_{\mathrm{n}})\rangle}\langle\sigma_{\mathrm{Re}}(E_{\mathrm{n}})\rangle, \tag{13}$$

where $\langle\sigma_{\mathrm{Au}}(E_{\mathrm{n}})\rangle$ and $\langle\sigma_{\mathrm{Re}}(E_{\mathrm{n}})\rangle$ are the experimental values measured in this paper and $\sigma_{\mathrm{Au}}(E_{\mathrm{n}})$ is the evaluated value obtained from the ENDF/B-VIII.0 database. Finally, the results of the cross section of rhenium in the continuum region from 2 to 300 keV are given in 20 bins per decade and are listed in Table III.

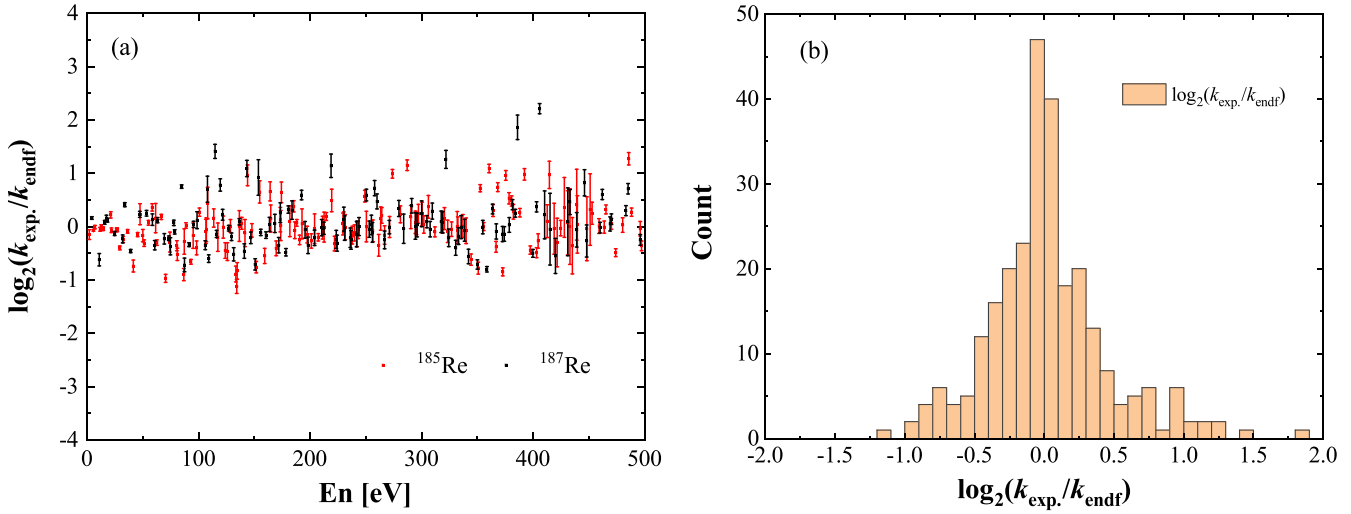

FIG. 13. (a) Logarithmic capture kernel ratios obtained from ENDF/B-VIII.0 database [14] k_{endf} and the present experimental results $k_{\mathrm{exp.}}$ as a function of the resonance energy. (b) Corresponding statistical distribution of these logarithmic ratios.

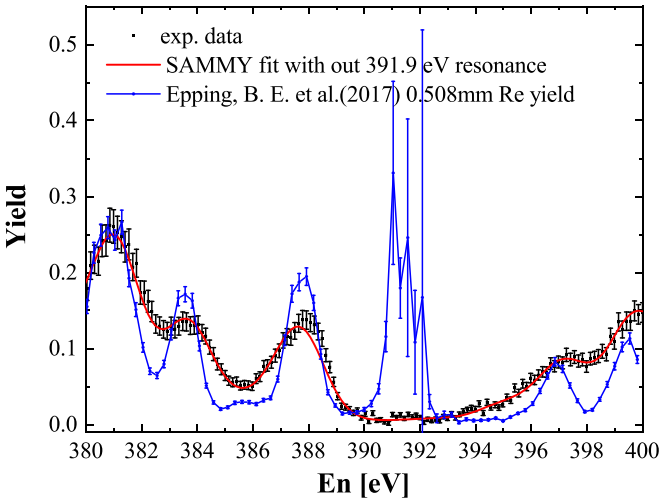

FIG. 14. Comparison of yield near 391.9 eV resonance between this paper and values of 0.508 mm rhenium target measured by Epping *et al.* (2017) in RPI LINAC [4].

In Fig. 17(a), the averaged cross sections obtained in this work in the continuum region are compared with previous experimental results and the evaluated database. Our measurements are consistent with TENDL 2019.s60 [16] in the 10–400 keV region, while a clear discrepancy is observed in the 2–10 keV range. All measured points lie in between the JEFF 3.3 [17], ENDF/B-VIII.0, and JENDL-5 [15] evaluated databases, and they basically agree with these databases within the uncertainty range. Over the past few decades, ten experiments have been performed to measure the averaged capture cross section of natural rhenium in the URR region. Good agreement is found between our work and the values obtained by Block *et al.* (1961) [11] and Bergman *et al.* (1971) [13], while our values are significantly higher than those reported by Kononov *et al.* (1965) [18] and Voignier *et al.* (1992) [23]. For comparison, we illustrated capture cross section of rhenium calculated with neutron flux determined by Li–Si detector (black dots) and the result measured relative to the gold sample in Fig. 17(b). In the region over 200 keV, the Li–Si detector determined result is obviously higher than the result measured relative to the gold sample. Near 30 keV, the fluctuation of the result determined by the Li–Si detector is caused by aluminum material in the neutron beam pipe.

The TALYS code was used to describe the isotopic average cross sections in the URR. The calculations were based on the Hauser–Feshbach statistical emission model, which assumes that the capture reactions occur by means of a compound nuclear systematic that reaches a statistical equilibrium. The previous obtained statistical average level space D_0 average radiation width $\langle\Gamma_\gamma\rangle$ were used as input parameters for the TALYS code calculations. In addition, the global neutron optical model potential of Ref. [54] was used in the calculations and other parameters are chosen with the method reported in Chen *et al.* (2020) [55], photon strength function is given by Kopecky and Uhl [56], level density a and nuclear temperature T are given by the Gilbert-Cameron model with adjusted parameters. In addition, $\langle\Gamma_\gamma\rangle$ is systematically multiplied by a factor of 1.2 for both isotopes to obtain the γ transmission coefficient. The calculated capture cross sections well reproduced the available experimental average cross sections of ^{185}Re and ^{187}Re, as illustrated in Figs. 18(a) and 18(b). From these averaged cross-section values, the MACSs of ^{185}Re and ^{185}Re were calculated for thermal energies kT from 5 to

TABLE III. Averaged capture cross sections of natural rhenium in the URR.

E_{low} (keV)	E_{up} (keV)	σ_{Re}(mb)	E_{low} (keV)	E_{up} (keV)	σ_{Re}(mb)
2.0	2.3	9059.4 ± 805.7	27.2	30.8	1333.0 ± 147.9
2.3	2.6	9957.2 ± 885.4	30.8	34.9	1297.7 ± 121.5
2.6	2.9	9076.5 ± 807.0	34.9	39.5	1135.6 ± 125.5
2.9	3.3	7881.5 ± 700.9	39.5	44.7	1080.9 ± 113.2
3.3	3.7	7523.1 ± 668.9	44.7	50.6	1041.8 ± 98.1
3.7	4.2	6106.3 ± 543.2	50.6	57.3	959.2 ± 99.3
4.2	4.8	6656.9 ± 592.0	57.3	64.9	931.7 ± 89.0
4.8	5.4	5206.6 ± 470.9	64.9	73.5	833.0 ± 82.7
5.4	6.1	3775.3 ± 460.5	73.5	83.3	829.6 ± 78.9
6.1	6.9	4174.7 ± 425.4	83.3	94.3	790.4 ± 85.8
6.9	7.8	3586.2 ± 382.4	94.3	106.8	741.8 ± 79.0
7.8	8.9	3348.1 ± 357.8	106.8	120.9	722.6 ± 74.0
8.9	10.1	2730.9 ± 313.9	120.9	136.9	693.7 ± 64.2
10.1	11.4	2588.1 ± 280.4	136.9	155.0	606.2 ± 64.0
11.4	12.9	2445.1 ± 255.8	155.0	175.5	574.9 ± 61.8
12.9	14.6	2218.4 ± 217.4	175.5	198.7	542.5 ± 53.2
14.6	16.6	1937.0 ± 203.2	198.7	225.0	514.4 ± 52.5
16.6	18.7	1861.3 ± 195.1	225.0	254.8	445.1 ± 51.1
18.7	21.2	1703.9 ± 184.5	254.8	288.5	444.0 ± 46.2
21.2	24.0	1577.5 ± 159.2	288.5	326.7	357.3 ± 44.3
24.0	27.2	1440.6 ± 126.0	–	–	–

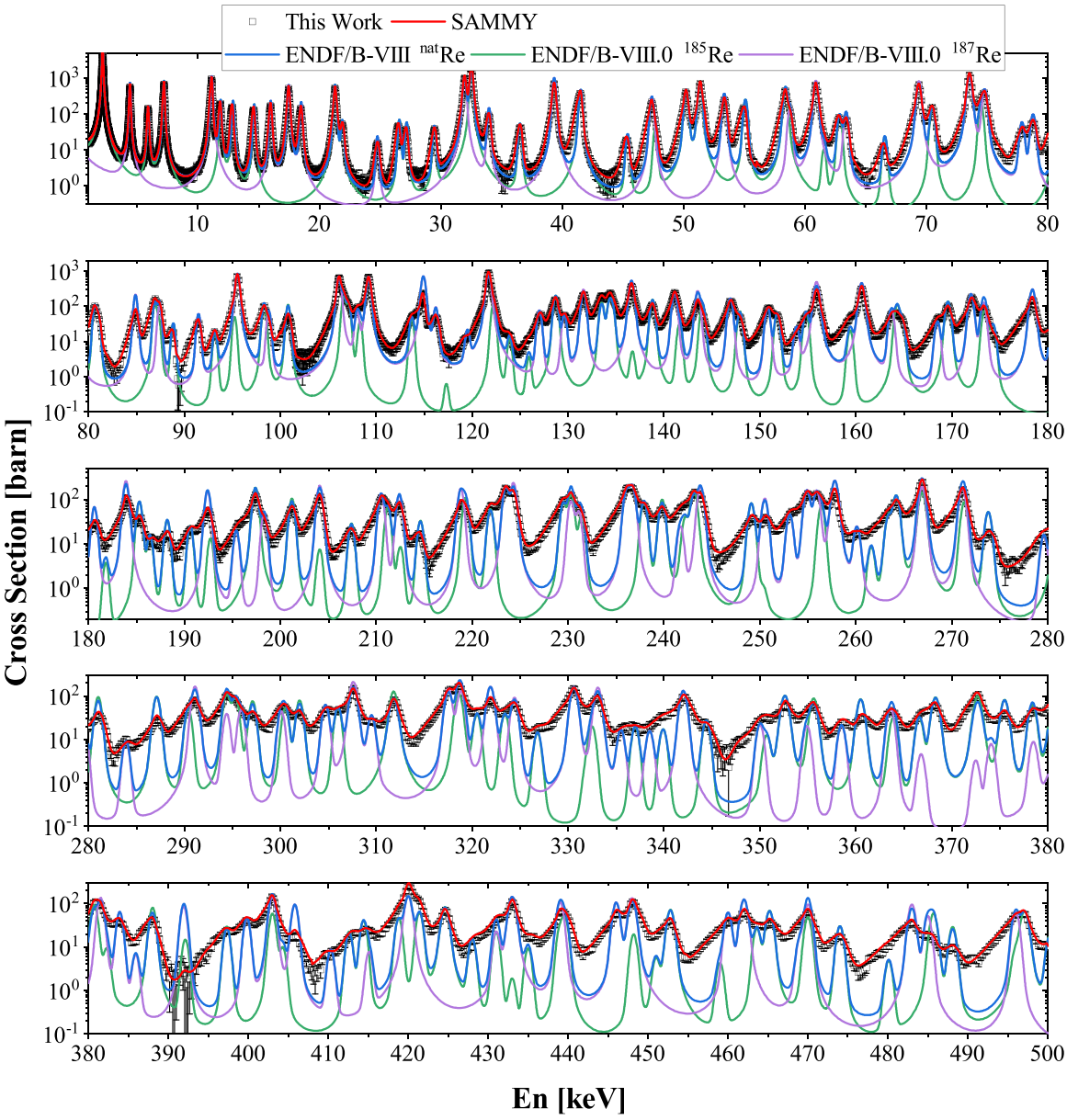

FIG. 15. Capture cross section $\sigma_{\text{exp.}}(\text{n},\gamma)$ calculated from the experimental yields obtained in this paper (black dots), SAMMY fitted results (red solid line), and evaluated databases ENDF/B-VIII.0 are plotted for comparison.

100 keV according to

$$\langle\sigma\rangle_{kT} = \frac{2}{\sqrt{\pi}} \frac{\int_0^\infty \sigma(E_n) E_n \mathrm{e}^{-E_n/kT}\,\mathrm{d}E_n}{\int_0^\infty E_n \mathrm{e}^{-E_n/kT}\,\mathrm{d}E_n}, \tag{14}$$

and the corresponding results are listed in Table IV. Figure 19 shows the comparison of our results, the evaluated databases, and the recommended values compiled in the Karlsruhe Astrophysical Database of Nucleosynthesis in Stars (KADoNiS) [57]: (a) the MACS values of ^{185}Re obtained in this paper, which are basically located between the values of the JEFF-3.3, TENDL 2019.s60, ENDF/B-VIII.0, and JENDL-5 databases, are in good agreement with the KADoNiS values; and (b) for ^{187}Re, the calculated values are considerably higher than those of the evaluated database and the KADoNiS recommended values.

Figure 20 shows the comparison of our results and the previously obtained MACSs at the nuclear astrophysics concerned thermal energy of $kT = 30$ keV. The value of 1469 ± 127 mb for ^{185}Re shown in Fig. 20(a) is in good agreement with the KADoNiS [57] recommended value of 1439 ± 58 mb [61] within the uncertainty range. On the other hand, the MACS value of 1361 ± 118 mb for ^{187}Re shows a discrepancy with the KADoNiS recommend value of 1184 ± 60 mb, lying between the points of AGM71 [62], HWF76 [63], and Har81 [64], KJB91 [61].

V. CONCLUSIONS

The (n,γ) reaction of natural rhenium was measured at the Back-n facility of CSNS with the aim of improving the accuracy of the neutron capture cross section in the RRR and the

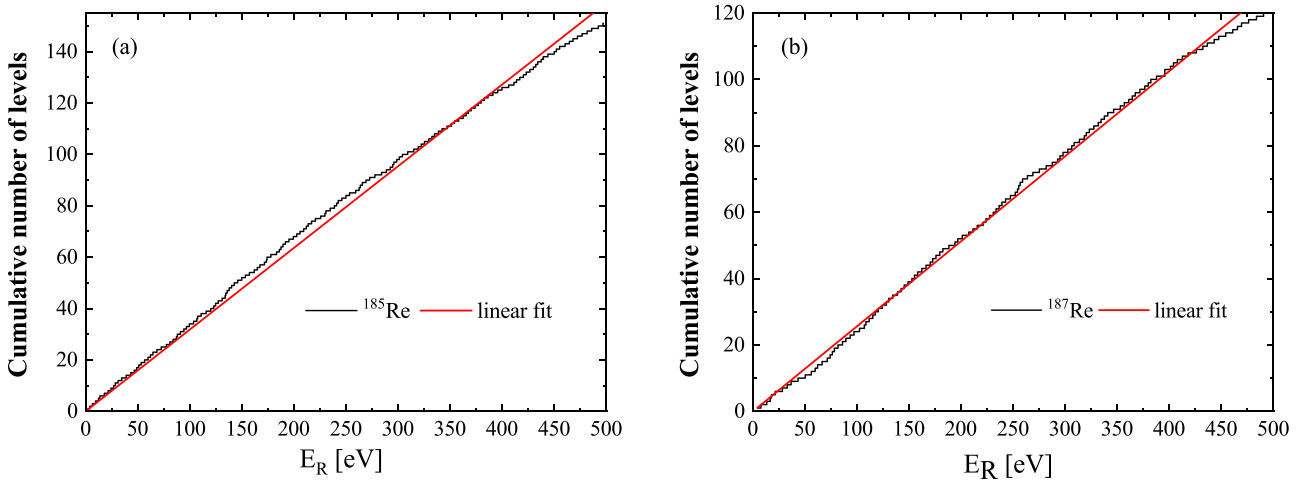

FIG. 16. Staircase plots of the cumulative numbers of resonances in the investigated energy region for rhenium isotopes.

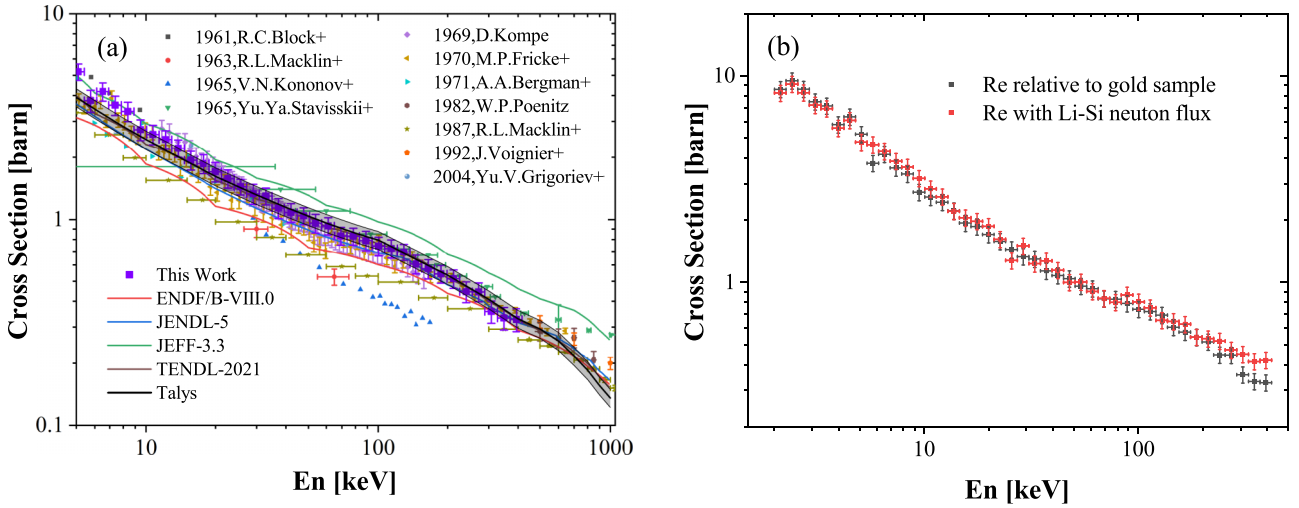

FIG. 17. (a) Capture cross sections of rhenium measured in this work relative to the ^{197}Au sample (red square dots). Previous measured values include data by Macklin *et al.* (1963) [12], Kononov *et al.* (1965) [18], Stavisskii *et al.* (1965) [19], Friesenhahn *et al.* (1968) [20], Kompe (1969) [21], Friesenhahn *et al.* (1970) [22], Macklin and Young (1987) [5], Voignier *et al.* (1992) [23], Block *et al.* (1961) [11], and Bergman *et al.* (1971) [13]. The theoretical averaged cross sections of natural rhenium obtained using the TALYS code are shown in black solid line. (b) Comparison between capture cross section of rhenium relative to gold (red dots) and result calculated with neutron flux determined by Li–Si detector (black dots).

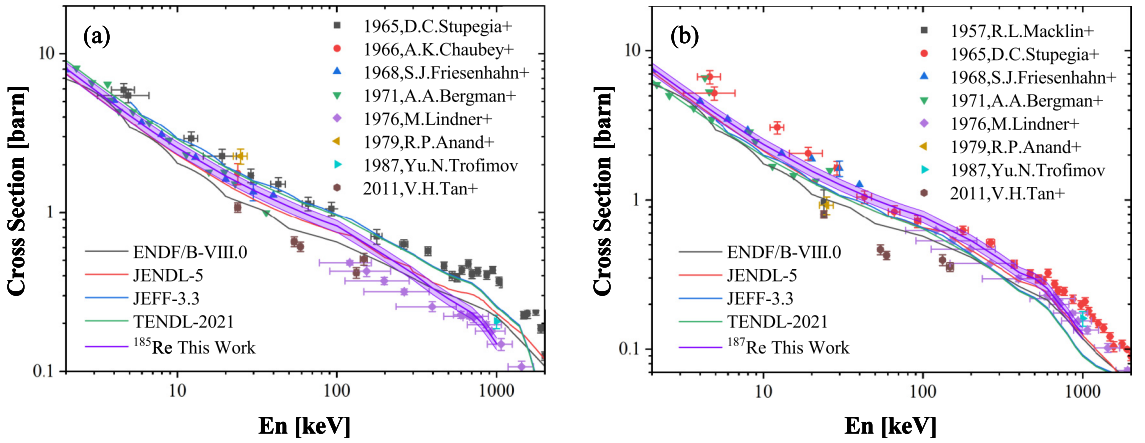

FIG. 18. Averaged capture cross sections of ^{185}Re(a) and ^{187}Re(b) calculated using the TALYS code. The theoretical averaged cross sections of ^{185}Re are basically consistent with the previous measurements and evaluated values, while those of ^{187}Re roughly agree with the previous experimental results but are higher than those of the evaluated database.

TABLE IV. MACSs of ^{185}Re and ^{187}Re.

	^{185}Re		^{187}Re	
kT (keV)	This work (mb)	KADoNiS v1.0 (mb)	This paper (mb)	KADoNiS v1.0 (mb)
5	3951 ± 343	4650 ± 416	3686 ± 320	3755
10	2665 ± 231	2815 ± 224	2471 ± 214	2378
15	2121 ± 184	2150 ± 150	1962 ± 170	1797
20	1814 ± 157	1804 ± 108	1677 ± 145	1494
25	1613 ± 140	1588 ± 80	1493 ± 129	1309
30	1469 ± 127	1439 ± 58	1361 ± 118	1184±60
40	1271 ± 110	1240 ± 56	1182 ± 102	1024
50	1135 ± 98	1112 ± 56	1061 ± 92	922
60	1034 ± 89	1021 ± 56	970 ± 84	849
80	885 ± 76	896 ± 58	837 ± 72	745
100	775 ± 67	812 ± 61	737 ± 64	672

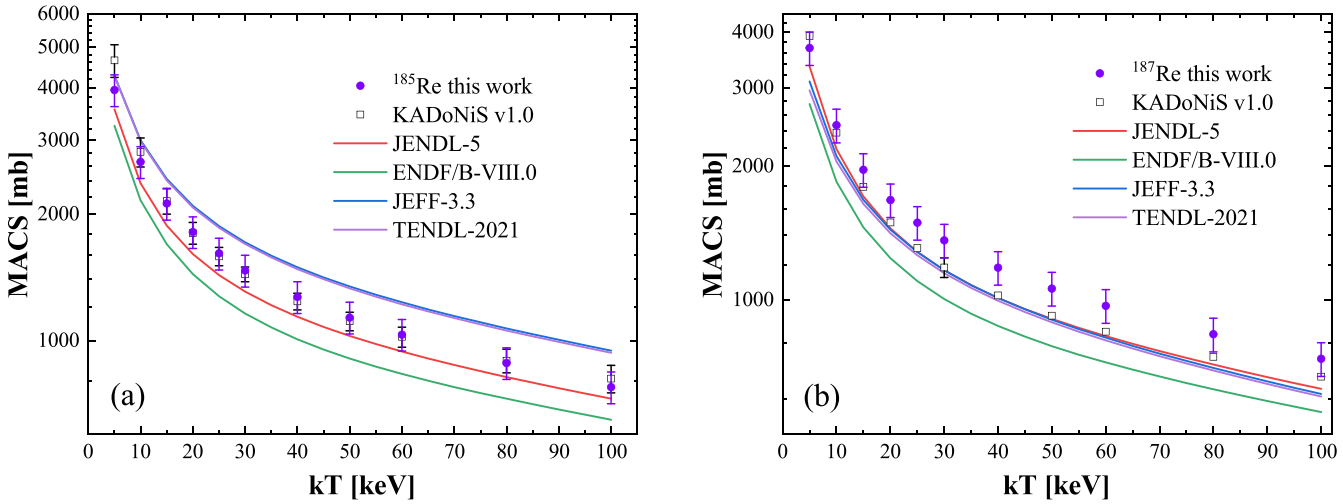

FIG. 19. MACSs calculated with Eq. (14) are illustrated in (a) and (b) for ^{185}Re and ^{187}Re, respectively.

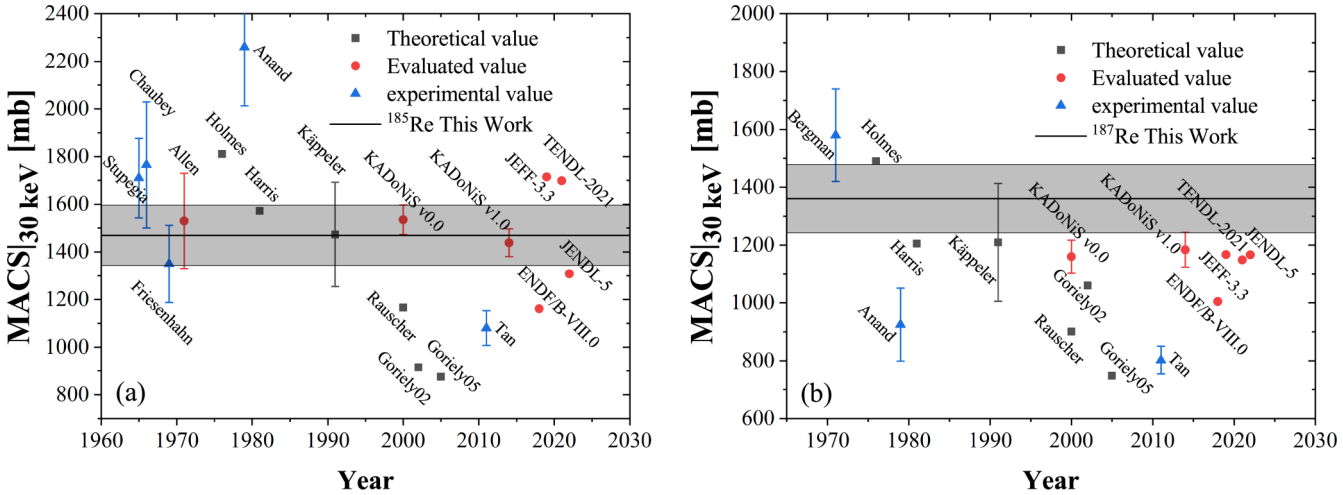

FIG. 20. MACSs at the thermal energy of $kT = 30$ keV for (a) ^{185}Re and (b) ^{185}Re. The results from the present paper are indicated by the gray-shaded areas. The solid blue triangles represent previous experimental results, namely, Anand *et al.* [58], Tan *et al.* [59], and Chaubey and Sehgal [60]. The theoretical values are indicated by the solid black squares from Käppeler *et al.* [61], Holmes *et al.* [63], Harris [64], and Rauscher and Thielemann [65]. The recommended values of the evaluated databases are indicated by solid red circles, which include the following works: Allen *et al.* [62], KADoNiS [57], ENDF/B-VIII.0 [14], TENDL-2021 [16], JENDL-5 [15], and JEFF-3.3 [17].

URR. A total energy systematic based on hydrogen-free C_6D_6 liquid scintillators was employed to detect the cascade γ rays. The PHWT and the double-bunch unfolding method were used for the data preprocessing; they were developed for the Back-n setup. A black resonance method with a Ta–Ag–Co filter was used to determine the backgrounds. Corrections obtained from GEANT4 simulations were applied to account for neutron multiple scattering events and neutron self-shielding in the URR.

The resonances were analyzed using the SAMMY code to extract the radiative kernels. A total of 270 resonances were found in the neutron energy range from 1 to around 500 eV, and an absence of 391.9 eV resonance is found in the analysis. In the URR, the average cross sections of natural rhenium measured relative to ^{197}Au were reported in logarithmical equidistant energy bins with 20 bins per energy decade. For thermal energies kT from 5 to 100 keV, the average cross sections of ^{185}Re and ^{187}Re were given by the TALYS code calculation. The MACSs for ^{185}Re obtained in this paper are basically located between the JEFF-3.3, TENDL 2019.s60, and ENDF/B-VIII.0 JENDL-5 databases, and they are in good agreement with the KADONIS values [57]. By contrast, for ^{187}Re, the calculated values are substantially higher than those of the evaluated database and the KADONIS recommended values. The MACSs at $kT = 30$ keV are 1469 ± 127 and 1361 ± 118 mb for ^{185}Re and ^{187}Re, respectively. In particular, the value for ^{187}Re obtained in this paper is considerably higher than the KADONIS recommend value. Our results provide additional constraints on the actual MACSs of ^{185}Re and ^{187}Re.

ACKNOWLEDGMENTS

We are grateful to the members of the CSNS Back-n Collaboration for enlightening discussions. This work was supported by the National Natural Science Foundation of China (Grants No. U1832182, No. 11875328, No. 11761161001, and No. U2032137), the Natural Science Foundation of Guangdong Province, China (Grants No. 18zxxt65 and No. 2022A1515011184), the Science and Technology Development Fund, Macau SAR (Grant No. 008/2017/AFJ), the Macao Young Scholars Program of China (Grant No. AM201907), the China Postdoctoral Science Foundation (Grants No. 2016LH0045 and No. 2017M621573), and the Fundamental Research Funds for the Central Universities (Grants No. 22qntd3101 and No. 2021qntd28).

[1] W. M. Haynes, D. R. Lide, and T. J. Bruno, *CRC Handbook of Chemistry and Physics*, 95th ed. (CRC Press, Inc., Boca Raton, 2014).

[2] S. Nogami, A. Hasegawa, M. Fukuda, S. Watanabe, J. Reiser, and M. Rieth, Tungsten modified by potassium doping and rhenium addition for fusion reactor applications, Fusion Eng. Des. **152**, 111445 (2020).

[3] S. Nogami, D. Terentyev, A. Zinovev, C. Yin, M. Rieth, G. Pintsuk, and A. Hasegawa, Neutron irradiation tolerance of potassium-doped and rhenium-alloyed tungsten, J. Nucl. Mater. **553**, 153009 (2021).

[4] B. E. Epping, G. Leinweber, D. P. Barry, M.J. Rapp, R. C. Block, T. J. Donovan, Y. Danon, and S. Landsberger, Rhenium resonance parameters from neutron capture and transmission measurements in the energy range 0.01 eV to 1 keV, Prog. Nucl. Energy **99**, 59 (2017).

[5] R. L. Macklin and P. G. Young, Neutron capture cross sections of rhenium from 3 to 1900 keV, Nucl. Sci. Eng. **97**, 239 (1987).

[6] M. Galeazzi, F. Fontanelli, F. Gatti, and S. Vitale, End-point energy and half-life of the ^{187}Re β decay, Phys. Rev. C **63**, 014302 (2000).

[7] D. D. Clayton, Cosmoradiogenic chronologies on nucleosynthesis, Astrophys. J. **139**, 637 (1964).

[8] M. Mosconi, K. Fujii, A. Mengoni, C. Domingo-Pardo, F. Käppeler, U. Abbondanno, G. Aerts, H. Álvarez-Pol, F. Alvarez-Velarde, S. Andriamonje *et al.*, Neutron physics of the Re/Os clock. I. Measurement of the (n, γ) cross sections of ^{186,187,188}Os at the CERN n TOF facility, Phys. Rev. C **82**, 015802 (2010).

[9] A. D. Brandon, M. Humayun, I. S. Puchtel, I. Leya, and M. Zolensky, Osmium isotope evidence for an s-process carrier in primitive chondrites, Science **309**, 1233 (2005).

[10] T. Hayakawa, T. Shizuma, T. Kajino, S. Chiba, N. Shinohara, T. Nakagawa, and T. Arima, New s-process path and its implications for a ^{187}Re - ^{187}Os nucleo-cosmochronometer, Astrophys. J. **628**, 533 (2005).

[11] R. C. Block, G. G. Slaughter, L. W. Weston, and F.C.Vonderlage, Neutron radiative capture measurements utilizing a large liquid scintillator detector at the ornl fast chopper, *Conf: Time of Flight methods Conf.* (Saclay, Oak Ridge, TN, 1961), p. 203.

[12] R. L. Macklin, J. H. Gibbons, and T. Inada, Average radiative capture cross sections for 30-and 65-keV neutrons, Phys. Rev. **129**, 2695 (1963).

[13] A. A. Bergman, D. K. Kaipov, V. A. Konks, and S. A. Romanov, Radiative capture of neutrons by rhenium isotopes, *Conf: Neutron Physics Conf.* (Kiev, 1971), Vol. 1, p. 144.

[14] D. A. Brown, M. B. Chadwick, R. Capote, A. C. Kahler, A. Trkov, M. W. Herman, A. A. Sonzogni, Y. Danon, A. D. Carlson, M. Dunn *et al.*, ENDF/B-VIII.0: The 8th major release of the nuclear reaction data library with CIELO-project cross sections, new standards and thermal scattering data, Nucl. Data Sheets **148**, 1 (2018).

[15] O. Iwamoto, N. Iwamoto, S. Kunieda, F. Minato, S. Nakayama, Y. Abe, K. Tsubakihara, S. Okumura, C. Ishizuka, T. Yoshida *et al.*, Japanese evaluated nuclear data library version 5: JENDL-5, J. Nucl. Sci. Technol. **60**, 1 (2023).

[16] A. J. Koning, D. Rochman, J. C. Sublet, N. Dzysiuk, M. Fleming, and S. van der Marck, TENDL: Complete nuclear data library for innovative nuclear science and technology, Nucl. Data Sheets **155**, 1 (2019).

[17] A. J. M. Plompen, O. Cabellos, D. S. C. Jean, M. Fleming, A. Algora, M. Angelone, P. Archier, E. Bauge, O. Bersillon, A. Blokhin *et al.*, The joint evaluated fission and fusion nuclear data library, JEFF-3.3, Eur. Phys. J. A **56**, 181 (2020).

[18] V. Kononov, Y. Y. Stavisskii, V. Kolesov, Rept: Fiz-Energ Institut, Obninsk Reports. No. 29 (1965).

[19] Y. Y. Stavisskii, A. V. Shapar, and R. N. Krasnokutskii, Fast neutron capture cross section for rhenium, Sov. At. Energy **19**, 905 (1965).

[20] S. J. Friesenhahn, D. A. Gibbs, E. Haddad, and F.H.frohner, Neutron capture cross sections and resonance parameters of rhenium from 0.01 eV to 30 keV, J. Nucl. Energy **22**, 191 (1968).

[21] D. Kompe, Capture cross-section measurements of some medium-and heavy-weight nuclei in the keV region, Nucl. Phys. A **133**, 513 (1969).

[22] S. J. Friesenhahn, M. P. Fricke, D. G. Costello, W. M. Lopez, and A. D. Carlson, Neutron resonance parameters and radiative capture cross section of Gd from 3 eV to 750 keV, Nucl. Phys. A **146**, 337 (1970).

[23] J. Voignier, S. Joly, and G. Grenier, Capture cross sections and gamma-ray spectra from the interaction of 0.5- to 3.0-MeV neutrons with nuclei in the mass range A = 45 to 238, Nucl. Sci. Eng. **112**, 87 (1992).

[24] H. Chen and X. L. Wang, China's first pulsed neutron source, Nat. Mater. **15**, 689 (2016).

[25] Q. An, H. Y. Bai, J. Bao, P. Cao, Y. Chen, Y. L. Chen, P. J. Cheng, R. R. Fan, C. Q. Feng, J. Gu *et al.*, Back-n white neutron facility for nuclear data measurements at CSNS, J. Inst. **12**, P07022 (2017).

[26] J. Ren, X. Ruan, J. Bao, G. Y. Luan, W. Jiang, Q. An, H. Y. Bai, P. Cao, Q. P. Chen, Y. H. Chen *et al.*, The C_6D_6 detector system on the Back-n beam line of CSNS, Radiat. Detect. Technol. Meth. **3**, 52 (2019).

[27] Q. Li, G. Luan, J. Bao, J. Y Tang, H. T. Jing, R. R. Fan, H. Y. Bai, W. Jiang, C. J. Ning, J. Ren *et al.*, The ^{6}LiF-silicon detector array developed for real-time neutron monitoring at white neutron beam at CSNS, Nucl. Instrum. Methods Phys. Res. Sect. A **946**, 162497 (2019).

[28] N. Larson, Updated users' guide for SAMMY multilevel R-matrix fits to neutron data using Bayes' equation, Report No. ORNL/TM-9179/R6, Oak Ridge National Laboratory, USA (2003).

[29] R. L. Macklin, J. Halperin, and R. R. Winters, Absolute neutron capture yield calibration, Nucl. Instrum. Methods **164**, 213 (1979).

[30] A. J. Koning, S. Hilaire, and S. Goriely, TALYS: modeling of nuclear reactions, Eur. Phys. J. A **59**, 131 (2023).

[31] S. Goriely, S. Hilaire, and A. J. Koning, Improved predictions of nuclear reaction rates with the TALYS reaction code for astrophysical applications, Astron. Astrophys. **487**, 767 (2008).

[32] J. Tang, Q. An, J. Bai, J. Bao, Y. Bao, P. Cao, H. L. Chen, Q. P Chen, Y. H. Chen, Z. Chen *et al.*, Back-n white neutron source at CSNS and its applications, Nucl. Sci. Tech. **32**, 11 (2021).

[33] X. X. Li, L. X. Liu, W. Jiang, J. Ren, H. W. Wang, G. T. Fan, X. G. Cao, Y. Zhang, X. R. Hu, Z. R. Hao, P. Kuang, B. Jiang, X. H. Wang, J. F. Hu, J. C. Wang, D. X. Wang, S. Y. Zhang, Y. D. Liu, X. Ma, C. W. Ma, Y. T. Wang, Z. D. An, J. J. He, J. Su, L. Y. Zhang, Y. X. Yang, W. B. Liu, and W. Q. Su, New experimental measurement of ^{nat}Er (n, γ) cross sections between 1 and 100 eV, Phys. Rev. C **104**, 054302 (2021).

[34] X. X. Li, L. X. Liu, W. Jiang, J. Ren, H. W. Wang, G. T. Fan, D. X. Wang, S. Y. Zhang, G. L. Yang, X. K. Li, Z. D. An, J. J. He, W. Luo, X. G. Cao, L. L. Song, Y. Zhang, X. R. Hu, Z. R. Hao, P. Kuang, B. Jiang, X. H. Wang, J. F. Hu, Y. D. Liu, C. W. Ma, Y. T. Wang, J. Su, L. Y. Zhang, Y. X. Yang, S. Feng, W. B. Liu, W. Q. Su, S. Jin, and K. J. Chen, Experimental determination of the neutron resonance peak of ^{162}Er at 67.8 eV, Phys. Rev. C **106**, 065804 (2022).

[35] X. K. Li, Z. D. An, W. Jiang, G. L. Yang, W. W. Qiu, Z. F. Liao, Z. Y. Zhuang, X. P. Zhang, S.L. Chen, C. C. Guo *et al.*, Measurement of the ^{nat}Eu(n, γ) cross section up to 500 keV at the CSNS Back-n facility, and the stellar ^{151,153}Eu(n, γ) cross section at s-process temperatures, Eur. Phys. J. A **58**, 251 (2022).

[36] X. K. Li, Z. D. An, W. Jiang, J. Y. Zhang, R.R. Bai, S. K. Liu, X. X. Li, Z. C. Zhu, G. L. Yang, W. W. Qiu *et al.*, Measurement of the ^{141}Pr cross section up to stellar s-process temperatures at the China Spallation Neutron Source Back-n facility, Phys. Rev. C **108**, 035802 (2023).

[37] Z. D. An, W. W. Qiu, W. Jiang, G. L. Yang, X. K. Li, Z. F. Liao, Z. Y. Zhuang, X. P. Zhang, S.L. Chen, C. C. Guo *et al.*, Measurement of the ^{181}Ta(n, γ) cross section up to stellar s-process temperatures at the CSNS Back-n, Sci. Rep. **13**, 12657 (2023).

[38] G. L. Yang, Z. D. An, W. Jiang X. K. Li, W. W. Qiu, Z. F. Liao, Z. Y. Zhuang, X. P. Zhang, S.L. Chen, C. C. Guo *et al.*, Measurement of Br(n, γ) cross sections up to stellar s-process temperatures at the CSNS Back-n, Nucl. Sci. Tech. **34**, 180 (2023).

[39] J. Allison, K. Amako, J. Apostolakis, P. Arce, M. Asai, T. Aso, E. Bagli, A. Bagulya, S. Banerjee, G. Barrand *et al.*, Recent developments in Geant4, Nucl. Instrum. Methods Phys. Res. Sect. A **835**, 186 (2016).

[40] C. Massimi, P. Koehler, S. Bisterzo, N. Colonna, R. Gallino, F. Gunsing, F. Käppeler, G. Lorusso, A. Mengoni, M. Pignatari *et al.*, Resonance neutron-capture cross sections of stable magnesium isotopes and their astrophysical implications, Phys. Rev. C **85**, 044615 (2012).

[41] X. Hu, L. Liu, W. Jiang, J. Ren, G. T. Fan, H. W. Wang, X. G. Cao, L. L. Song, Y. D. Liu, Y. Zhang *et al.*, New experimental measurement of ^{nat}Se (n, γ) cross section between 1 eV to 1 keV at the CSNS Back-n facility, Chin. Phys. B **31**, 080101 (2022).

[42] J. N. Wilson, B. Haas, S. Boyer, D Dassie, G Barreau, M Aiche, S Czajkowski, C. Grosjean, and A Guiral, Measurements of (n, γ) neutron capture cross-sections with liquid scintillator detectors, Nucl. Instrum. Methods Phys. Res. Sect. A **511**, 388 (2003).

[43] U. Abbondanno, G. Aerts, H. Alvarez, S. Andriamonje, A. Angelopoulos, P. Assimakopoulos, C.O. Bacri, G. Badurek, P. Baumann, F. Bečvář *et al.*, New experimental validation of the pulse height weighting technique for capture cross-section measurements, Nucl. Instrum. Methods Phys. Res. Sect. A **521**, 454 (2004).

[44] H. Yi, T. F. Wang, Y. Li, X. C. Ruan, J. Ren, Y. H. Chen, Q. Li, J. Wen, J. Y. Tang, Q. An *et al.*, Double-bunch unfolding methods for the Back-n white neutron source at CSNS, J. Instrum. **15**, P03026 (2020).

[45] G. D'Agostini, A multidimensional unfolding method based on Bayes' theorem, Nucl. Instrum. Methods Phys. Res. Sect. A **362**, 487 (1995).

[46] J. Ren, X. Ruan, W. Jiang, J. Bao, G. Y. Luan, Q. W. Zhang, H. X. Huang, Y. B. Nie, Z. G. Ge, Q. An *et al.*, Background

study for (n, γ) cross section measurements with C_6D_6 detectors at CSNS Back-n, Nucl. Instrum. Methods Phys. Res. Sect. A **985**, 164703 (2021).

[47] J. Ren, X. Ruan, Y. Chen, W. Jiang, J. Bao, G. Y. Luan, Q. W. Zhang, H. X. Huang, Z. H. Wang, Q. An *et al.*, In-beam gamma-rays of back-streaming white neutron source at China Spallation Neutron Source, Acta Phys. Sin. **69**, 172901 (2020).

[48] C. Massimi, C. Domingo-Pardo, G. Vannini, L. Audouin, C. Guerrero, U. Abbondanno, G. Aerts, H. Álvarez, F. Álvarez-Velarde *et al.*, ^{197}Au(n, γ) cross section in the resonance region, Phys. Rev. C **81**, 044616 (2010).

[49] S. F. Mughabghab, *Atlas of Neutron Resonances*, 5th ed. (Elsevier, New York, 2006).

[50] B. Jiang, J. Han, W. Jiang, J. F. Hu, X. H. Wang, J. G. Chen, and X. Z. Cai, Monte-Carlo calculations of the energy resolution function with Geant4 for analyzing the neutron capture cross section of ^{232}Th measured at CSNS Back-n, Nucl. Instrum. Methods Phys. Res. Sect. A **1013**, 165677 (2021).

[51] A. I. Namenson, Neutron resonances in ^{185}Re and ^{187}Re, Nucl. Phys. A **266**, 83 (1976).

[52] A. Laminack, J. C. Blackmon, A. Couture, J. P. Greene, M. Krtička, K. T. Macon, S. Mosby, C. Prokop, J. L. Ullmann, and S. Valenta, Measurement of neutron-capture cross sections of ^{70,72}Ge using the DANCE facility, Phys. Rev. C **106**, 025802 (2022).

[53] F. J. Dyson and M. L. Mehta, Statistical theory of the energy levels of complex systems. IV, J. Math. Phys. **4**, 701 (1963).

[54] A. J. Koning and J. P. Delaroche, Local and global nucleon optical models from 1 keV to 200 MeV, Nuclear Physics A **713**, 231 (2003).

[55] S. Chen, P. Tamagno, D. Bernard, P. Archier, and G. Noguere, From nuclear physics to displacement damage calculation and uncertainty propagation in CONRAD, Results in Phys. **17**, 103023 (2020).

[56] J. Kopecky and M. Uhl, Test of gamma-ray strength functions in nuclear reaction model calculations, Phys. Rev. C **41**, 1941 (1990).

[57] I. Dillmann, M. Heil, F. Käppeler, T. Rauscher, and F.-K. Thielemann, KADoNiS-The Karlsruhe astrophysical database of nucleosynthesis in stars, AIP Conf. Proceedings **819**, 123 (2006).

[58] R. P. Anand, M. L. Jhingan, D. Bhattacharya, and E. Kondaiah, keV-neutron capture cross-sections, Il Nuovo Cim. A **50**, 247 (1979).

[59] V. H. Tan, P. N. Son, T. T. Anh, and M. X. Trung, Capture cross section measurements of ^{185,187}Re with filtered neutron beams at the Dalat research reactor, J. Korean Phys. Soc. **59**, 1757 (2011).

[60] A. K. Chaubey and M. L. Sehgal, Test of statistical theory of nuclear reactions at 24 keV, Phys. Rev. **152**, 1055 (1966).

[61] F. Käppeler, S. Jaag, Z. Bao, and G. Reffo, THE s-process branchings at ^{185}W and ^{186}Re, Astrophys. J. **366**, 605 (1991).

[62] B. Allen, J. Gibbons, and R. Macklin, Nucleosynthesis and neutron-capture cross sections, Adv. Nucl. Phys. **4**, 205 (1971).

[63] J. A. Holmes, S. E. Woosley, W. A. Fowler, and B.A. Zimmerman, Tables of thermonuclear-reaction-rate data for neutron-induced reactions on heavy nuclei, At. Data Nucl. Data Tables **18**, 305 (1976).

[64] M. J. Harris, 30 keV (n, γ) cross-sections from the nuclear statistical model, Astrophys. Space Sci. **77**, 357 (1981).

[65] T. Rauscher, F. Thielemann, Astrophysical reaction rates from statistical model calculations, At. Data Nucl. Data Tables **75**, 1 (2000).